Available online at www.sciencedirect.com
SCIENCE DIRECT®
PERGAMON
Scripta Materialia 49 (2003) 459–465
Scripta MATERIALIA
www.actamat-journals.com

Measurement of residual-stress effect by nanoindentation on elastically strained (1 0 0) W

Yun-Hee Lee *, Dongil Kwon

School of Materials Science and Engineering, Seoul National University, San 56-1, Shinrim-Dong, Gwanak-Gu, Seoul 151-742, South Korea

Received 28 January 2003; received in revised form 13 May 2003; accepted 15 May 2003

Abstract

The effects of elastic in-plane stress on surface-normal contact deformation were investigated by nanoindentation experiments on artificially strained (1 0 0) tungsten single crystal. Indentation-depth-controlled stress relaxation combined with a shear plastic-deformation concept is suggested to explain the stress-induced change in shape in the nanoindentation curve.

Keywords: Tungsten single crystal; Nanoindentation; Residual stresses; Stress interaction

1. Introduction

Nanoindentation is used to evaluate the mechanical properties of thin films because indenter penetration as shallow as a few nanometers suffices. In addition, thin films are often subjected to large residual stress due to the interfacial constraint [1]. Thus, the development of a methodology for characterizing thin-film stress by nanoindentation has became an important research issue. A generally observed effect of residual stress on the nanoindentation test is the shape change in the resulting curve corresponding to any stress state [2–4]. The indentation loading curve has a lower slope in the tensilely stressed state than in the stress-free state and a higher slope in the compressively stressed state; in other words, the indentation load of the unstressed state indented to a given depth increases or decreases under compressive or tensile stress, respectively. Numerous studies [2–4] have attempted to drive an empirical relationship between thin-film stress and hardness estimated from conventional unloading-curve analysis [5]. However, the alteration in the hardness by the elastic residual stress was less than 10% of its value in the unstressed specimen, so that the use of the hardness as a parameter of the residual stress is dubious.

Tsui et al. [6], studying the influence of in-plane stress on indentation plasticity by investigating both the shape of the indentation curve and the remnant contact impressions, reported that hardness was invariant regardless of the applied stress; this was supported by subsequent finite element analysis [7]. The FEA results showed the important role of sink-in or pile-up deformations around

* Corresponding author. Tel.: +82-2-8808025; fax: +82-2-8894380.
E-mail address: uni44@mmrl.snu.ac.kr (Y.-H. Lee).

1359-6462/03/$ - see front matter
doi:10.1016/S1359-6462(03)00290-2

the contact in the stressed state in producing this stress-insensitive hardness. A sharp indentation model for characterizing the residual stress proposed by Suresh and Giannakopoulos [8] treats the equi-biaxial thin-film stress as the sum of hydrostatic stress and differential contact stress along the indentation axis. Finally, the difference in contact area of stressed and unstressed materials at the same indentation depth was related to the residual stress. Other researchers [9] also reported the usefulness of the contact area ratio as a parameter indicating residual stress. The differential contact stress, however, still includes a plastic-deformation-independent hydrostatic stress and direct measurement of the contact area for each stress state is troublesome procedure. Taljat and Pharr [10] have recently suggested that nanoindentation with a spherical indenter can reveal more clear stress effects. Swadener et al. [11] proposed contact pressure at initial yielding as a stress indicator by analyzing the elastic and elastic/plastic deformations beneath the spherical indenter.

In this study, we explore a new stress-analysis technique for sharp nanoindentation by considering the stress interaction between the residual stress and the contact pressure from the viewpoint of the shear plasticity. The continuous changes in contact morphology and indentation load during stress relaxation are incorporated into the analysis.

2. Theoretical model

Elastic thin-film stress is taken as equi-biaxial in-plane state ($\sigma_{res,x} = \sigma_{res,y} = \sigma_{res}$, $\sigma_{res,z} = 0$) [1,8] and is separated into mean stress σ^M (hydrostatic stress) and plastic-deformation-sensitive shear deviator stress σ^D:

$$\underbrace{\begin{pmatrix} \sigma_{res} & 0 & 0 \\ 0 & \sigma_{res} & 0 \\ 0 & 0 & 0 \end{pmatrix}}_{\text{Thin-film stress}} = \underbrace{\begin{pmatrix} \frac{2}{3}\sigma_{res} & 0 & 0 \\ 0 & \frac{2}{3}\sigma_{res} & 0 \\ 0 & 0 & \frac{2}{3}\sigma_{res} \end{pmatrix}}_{\text{Mean stress part } (\sigma^M)} + \underbrace{\begin{pmatrix} \frac{1}{3}\sigma_{res} & 0 & 0 \\ 0 & \frac{1}{3}\sigma_{res} & 0 \\ 0 & 0 & -\frac{2}{3}\sigma_{res} \end{pmatrix}}_{\text{Deviator stress part } (\sigma^D)}. \quad (1)$$

The stress component along the indentation axis in the deviator stress part ($\sigma^D_{33} = -2\sigma_{res}/3$) is directly added to the surface-normal indentation pressure. Thus, the difference in the indentation load between stressed and unstressed specimens indented to a penetration depth is defined as a residual-stress-induced normal load, as expressed in Eq. (2):

$$L_{res} = -\frac{2}{3}\sigma_{res}A_C, \quad (2)$$

where A_C is the contact area between indenter and specimen. The sign and absolute magnitude of L_{res} are closely related to the residual stress. The differences in the indentation load and contact morphology of tensilely stressed and unstressed specimens are compared in Fig. 1. The decrease in the indentation load from L_0 to L_T by the tensile residual stress for the given depth h_t causes a proportional decrease in the contact area from A_C to A_C^T, satisfying the basic assumption of residual stress-independent hardness [6–8]. Thus, a significant contact feature under tensile stress compared

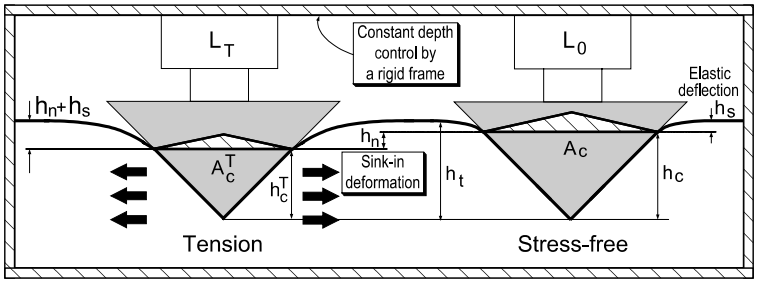

Fig. 1. Changes in contact morphology and indentation load during the indentation-depth-controlled continuous stress relaxation.

with the stress-free state is sink-in [12] or smaller pile-up deformation.

An indentation depth-controlled stress relaxation is investigated to evaluate residual stress σ_{res} quantitatively. We assumed reversible recoveries in the indentation load and the contact morphology by the stress relaxation. A gradual relaxation of the tensile stress (solid arrows in Fig. 1) causes a rebounding force that pushes the indenter out from the surface [12]. However, the rebounding force appears as the increases in the indentation load ($L_T \rightarrow L_0$) and the contact area ($A_C^T \rightarrow A_C$) because the indentation depth h_t is constrained by a rigid frame. Furthermore, the continuous stress relaxation is expressed as an integral equation in Eq. (3) with the definition of L_{res}.

$$L_0 = L_T + L_{res} = L_T - \frac{2}{3}\int_{L_T}^{L_0} d(\sigma \cdot A_C). \quad (3)$$

The continuous response of residual stress σ and contact area A_C during the stress relaxation must be expressed in the equations of the indentation load L to solve Eq. (3). The stress relaxation from the initial value of σ_{res} to the final stress-free state is assumed to be linear. If indentation size effects [13,14], which change the hardness in a broad sense, are removed, the contact area will be expressed as the indentation load divided by the hardness. However, the contact area is empirically fitted as an equation of the third degree in the indentation load under real nanoindentation tests. The fitting constants of the polynomial equation are given as R_0, R_1, R_2, and R_3. Finally, an equation for the elastic thin-film stress is derived from Eq. (3) by inserting the information on the contact area and stress variation during the depth-controlled continuous stress relaxation:

$$\sigma_{res} = \frac{3}{2}\frac{L_{res}^2}{R_3 L_T^4 + (R_2 - R_3 L_0)L_T^3 + (R_1 - R_2 L_0)L_T^2 + (R_0 - R_1 L_0)L_T - R_0 L_0}. \quad (4)$$

3. Experimental details

An isotropic tungsten single crystal was used in this study in order to exclude additive microstructure and anisotropic deformation effects on the nanoindentation curve. A (1 0 0) tungsten rod of diameter 10.0 mm and orientation error ±3° made by the Goodfellow Corporation was used in this study. Two types of 1.0 and 2.5 mm-thick disk specimens of diameter 8.0 mm were machined from the raw rod and were then mechanically ground and electrically polished in 2% NaOH aqueous solution at 6 V for 2 min. The roughness of the prepared surface measured by an atomic force microscope (Nanoscope II, made by Digital Instrument, Inc.) was 14.6 ± 3.5 nm.

The concentric bending and coercive inserting apparatuses in Fig. 2 were designed to generate equi-biaxial elastic tensile and compressive stresses, respectively. The concentric bending apparatus, similar in design to that in a previous study [11], consists of an outer supporting ring of diameter 6.0 mm (upper die) and an inner supporting ring of diameter 1.5 mm (lower die). The two dies with the 1.0 mm-thick specimen as a center plate were joined with a screw, as shown in Fig. 2(a). The elastically bent specimen has a stress gradient from tensile stress at the exposed convex surface to compressive stress at the concave bottom surface. The applied equi-biaxial tensile stress within a central circle of diameter 1.5 mm is uniform, and nanoindentation tests were done on this uniformly stressed area. Compressive stress was applied by coercively inserting the 2.5 mm-thick specimen into a rigid steel tube with smaller inner diameter. To facilitate the insertion process, the inside plane of the tube was obliquely machined with a tilting angle of 1° and the specimen thickness was increased to 2.5 mm to prevent warping. Finally, the specimen inserted at the middle of the original tube was cut from the tube, as illustrated in Fig. 2(b). The magnitude of the applied stress within elastic limit was measured by the strain gauge attached to the specimen surface. One tensile stress (Ten) and two compressive stress states (Com #1 and #2) were artificially generated using the aforementioned apparatuses.

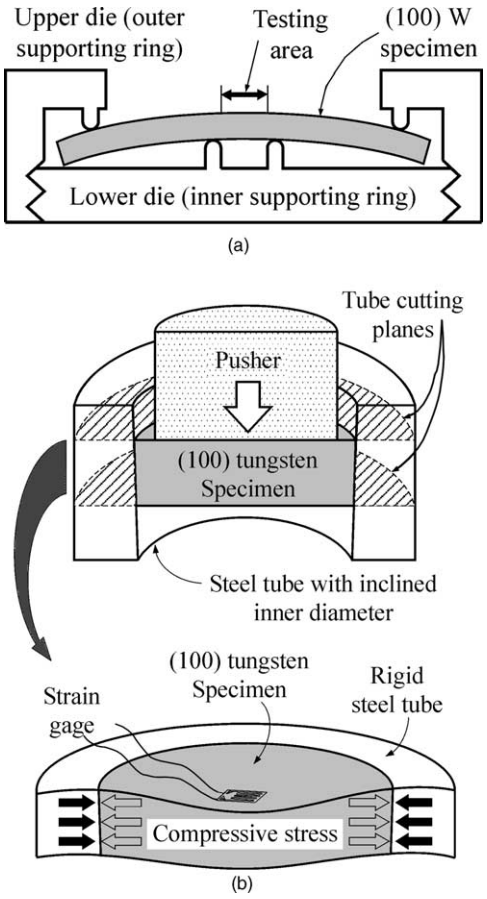

Fig. 2. Equi-biaxial tensile and compressive stresses are applied through (a) concentric bending and (b) coercive inserting apparatuses, respectively.

Nanoindentation tests on unstressed and stressed specimens were performed using Triboscope (made by Hysitron, Inc.) with depth and load resolutions of 0.1 nm and 0.1 μN, respectively. The indentation loads corresponding to the 1.0 and 2.5 mm-thick specimens were chosen as 5 and 10 mN, respectively. The indenter tip and indentation speed selected were respectively a three-sided pyramidal indenter and 250 μN/s. The indenter tip was also used as the imaging probe of the atomic force microscope and the specimen surface was imaged immediately before indentation in order to locate the indenter on the smoothest region. The artificially applied stress was effectively constant with indentation depth because the maximum penetration achieved by the indenter was less than 0.02% of specimen thickness. Careful system calibration and nanoindentation experiments were performed to obtain the nanoindentation results implying only the influences of mechanical stress applied to tungsten specimen. Also, more than ten nanoindentation tests were performed for an applied stress state to select one reliable representative indentation curve from the middle of the raw data.

4. Results and discussion

4.1. Effect of stress on the shape of the nanoindentation curve

The values of Young's modulus E and Poisson's ratio v of the (1 0 0) tungsten single crystal are 410 GPa and 0.28, respectively [15]. The measured strain from the strain gage attached on specimen surface was converted to applied stress by multiplying by a biaxial modulus or $E/(1-v)$. The artificial strains of $+3.943\times10^{-4}$, -3.882×10^{-4}, and -5.956×10^{-4} correspond to elastic applied stresses of +225, −221, and −339 MPa, respectively. Variation of the applied stress during the subsequent nanoindentation tests was less than ±0.57 MPa and negligible.

The measured indentation depth at 10 mN was reproducible within a standard deviation of ±1.7 nm regardless of stress state. Dotted lines in Fig. 3 represent the lower and upper location boundaries of the raw indentation curves from each stress state. The maximum indentation depths obtained from the ten superposed indentation curves for each stress state were also summarized in Table 1. The indentation curve corresponding to the tensile applied stress of +225 MPa (Ten) showed a shift to the right from the indentation curve for the stress-free state, while the indentation curves for the compressive applied stresses −221 (Com #1) and −339 MPa (Com #2) shifted to the left of that for the stress-free state. Since the indentation pressure is compressive and acts perpendicularly to the surface, the tensile applied stress increases the magnitude of the shear stress beneath the indenter relative to the unstressed specimen [6]. The in-

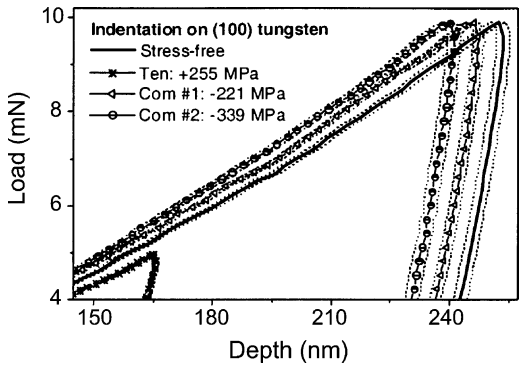

Fig. 3. Superposition of representative nanoindentation curves selected from approximately the central location of experimental results; dotted lines display the existing boundary of raw nanoindentation curves for each stress state.

crease of the shear stress under the tensile stress state enhances indentation plasticity, thereby producing a lower indentation load than in the stress-free state for the same indentation depth. By the same arguments, the effects of the compressive stress are expected to be symmetrically opposite to that of the tensile stress state. The nanoindentation tests on the unstressed specimens before and after the stress-generating tests formed perfect superposing indentation curves, proving that only elastic deformation occurred during the straining.

An indentation curve of the electropolished tungsten single crystal showed three regions of elastic, pop-in by abrupt dislocation movement, and subsequent elastic/plastic deformations. The indentation loading curves in the elastic region were superposed because the effect of the applied elastic stress on elastic indenting deformation is negligible. The critical indentation load for the pop-in showed no general dependency on the applied stress because such factors as surface roughness, crystalline defect density, and surface contaminants can also affect pop-in behavior [15,16].

4.2. Stress evaluation based on the theoretical relaxation model

The loading parts of the selected representative curves in Fig. 3 were fitted to the equation $L = k_L h^{m_L}$ to determine the integration limits in Eq. (3). L_0 and L_T are calculated by inserting a common indentation depth into the power-fitted equations in Table 1 for the unstressed and stress applied states, respectively.

According to the assumption of residual stress-insensitive hardness [6–8,12], there should be a unique contact area corresponding to a given indentation load. Thus, the contact area for the stress-free state, as evaluated through conventional unloading-curve analysis [5] or direct imaging of the contact impressions, is used as the unique contact area throughout this study regardless of the stress state. We measured the contact area as 2999184.8 ± 73395.2 nm^2 through the atomic force microscope; this is about 14.3% larger than that from Oliver and Pharr's unloading-curve analysis [5] because of the pile-up deformation around the residual indentation mark at 10 mN, as shown in Fig. 4. The reduced modulus E_r of a monolithic material was taken as an invariant intrinsic value regardless of the change in the indentation load or depth and expressed as

$$E_r = \frac{\sqrt{\pi}S}{2\sqrt{A_C}} = \frac{\sqrt{\pi}\omega L}{2(h - h_C)\sqrt{A_C}}, \quad (5)$$

where ω and h_C are a geometrical constant of an indenter and a contact depth, respectively. The reduced modulus calculated from Eq. (5) with the directly measured contact area and contact

Table 1
Scatter of maximum indentation depth in the raw nanoindentation results and power-law fitting equation for the representative loading curve for each stress state

Stress state (MPa)	Indentation depth (nm)	Fitted loading curves
Stress-free (0)	159.0 ± 1.10 (at 5 mN), 254.7 ± 1.71 (at 10 mN)	$L = 2.98\ h^{1.45}$
Ten (+225)	162.5 ± 0.80 (at 5 mN)	$L = 2.87\ h^{1.47}$
Com #1 (−221)	247.8 ± 1.41 (at 10 mN)	$L = 2.95\ h^{1.47}$
Com #2 (−339)	242.6 ± 1.71 (at 10 mN)	$L = 3.11\ h^{1.47}$

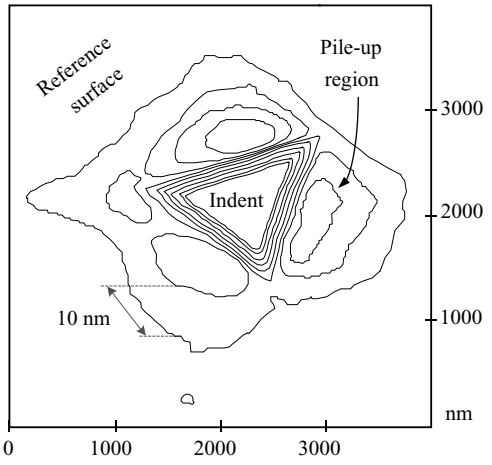

Fig. 4. Pile-up around the contact impression at 10 mN as seen with the atomic force microscope.

stiffness S obtained from the final unloading curve was 319.5 ± 5.2 GPa. The Young's modulus of the (1 0 0) tungsten monocrystal from the reduced modulus with the Poisson's ratio of 0.28 and elastic properties of the diamond indenter [5] was 408.4 ± 9.3 GPa, agreeing well with the value in the literature [15]. The right-hand side of Eq. (5) can be expressed as a function of the indentation load and contact depth because the contact area A_C is also a function of the contact depth h_C [5]. The reduced modulus calculated from Eq. (5) at a certain indentation load or depth was compared with the predetermined intrinsic value of 319.5 GPa. The contact depth at each selected load or depth was determined from the indentation depth yielding the same value as the predetermined reduced modulus. The contact area evaluated at each load step was expressed as the function of the indentation load in Table 2. The stresses for the elastically strained specimens, as evaluated by inserting the analyzed nanoindentation data into Eq. (4), are compared with the measured applied stresses in Table 3. The averaged stress from the nanoindentation stress-relaxation technique agreed well with the applied stress measured by the strain gauge (within a standard deviation of ±26.4 MPa). However, the analyzed stress from Eq. (4) using all nanoindentation results without averaging and selecting representative curve produced large scatter to within 25–35% of the applied stress because such suspicious factors as surface roughness or tilting, electropolishing-induced damage, contaminant or oxide layer, surface crystalline defect can also influence the shape of nanoindentation curve.

Table 3
Comparison of the stresses evaluated from the nanoindentation stress-relaxation technique and the measured applied values

Measured applied stress from strain gage (MPa)	Stresses from nanoindentation stress-relaxation technique (MPa)
+225	$+263.1 \pm 10.2$
−221	-225.2 ± 11.1
−339	-364.0 ± 14.7

5. Summary

Equi-biaxial in-plane stresses within the elastic limit were applied to (1 0 0) tungsten disks using specially designed apparatuses. A significant shape change in the nanoindentation curve was detected from the nanoindentation results for the three applied stress and stress-free states. The indentation load necessary to attain a given indentation

Table 2
Contact properties for the unstressed specimen measured and predicted from direct observation of the residual indentation impressions and the elastic contact assumption

Load (mN)	Indentation depth (nm)	Contact depth (nm)	Contact area (nm^2)
10	254.7 ± 1.71	242.0 ± 1.66	$2{,}999{,}184.8 \pm 73{,}395.2$
8	219.3 ± 1.46	207.5 ± 1.32	$1{,}846{,}477.5 \pm 46{,}974.4$
6	180.2 ± 1.21	169.1 ± 1.19	$1{,}174{,}530.9 \pm 28{,}705.5$
4	136.6 ± 0.90	126.9 ± 0.93	$679{,}263.3 \pm 17{,}504.6$

$A_C = 4.37 \times 10^{-6} L^3 - 0.05 L^2 + 442.69 L - 477017.97$

depth in the tensile stress state was lower than in the stress-free state because the plasticity was enhanced by the interaction of the in-plane tensile stress and the surface-normal indentation pressure. In addition, the contact morphology in the stressed state as modeled according to the basic assumption of residual-stress-independent hardness was compared with that of unstressed state. The difference in the indentation load in the stressed and unstressed states for a given indentation depth was defined as a residual-stress-induced normal load and was represented as the product of the contact area and a deviator stress component extracted from the equi-biaxial thin-film stress. Finally, an integral residual-stress-analysis equation was derived by describing continuous stress relaxation at a constant indentation depth with the aid of the residual-stress-induced normal load and was applied to confirm the stress by nanoindentation tests on the artificially strained (1 0 0) tungsten specimens. The residual stress from the proposed nanoindentation stress-relaxation technique agreed well with the applied stresses (within a standard deviation of ±26.4 MPa). Additionally, careful control of nanoindentation tests and sufficient data acquisition are necessary for assessing accurate stress value and for extracting only the effects of residual stress from the raw nanoindentation results also implying various subsidiary effects.

References

[1] Nix WD. Metall Trans A 1989;20A:2217.
[2] Zagrebelny AV, Carter CB. Scripta Mater 1997;37:1869.
[3] LaFontaine WR, Paszkiet CA, Korhonen MA, Li CY. J Mater Res 1991;6:2084.
[4] Doerner MF, Gardner DS, Nix WD. J Mater Res 1986;1:845.
[5] Oliver WC, Pharr GM. J Mater Res 1992;7:1564.
[6] Tsui TY, Oliver WC, Pharr GM. J Mater Res 1996;11:752.
[7] Bolshakov A, Oliver WC, Pharr GM. J Mater Res 1996;11:760.
[8] Suresh S, Giannakopoulos AE. Acta Mater 1998;46:5755.
[9] Carlsson S, Larsson PL. Acta Mater 2001;49:2179.
[10] Taljat B, Pharr GM. In: Vinci R, Kraft O, Moody N, Shaffer E, editors. Thin Films: Stresses and Mechanical Properties VIII. Pennsylvania, USA: Materials Research Society; 2000. p. 519–24.
[11] Swadener JG, Taljat B, Pharr GM. J Mater Res 2001;16:2091.
[12] Lee YH, Kwon D. J Mater Res 2002;17:901.
[13] Lu CJ, Bogy DB. Int J Solids Struct 1995;32:1759.
[14] Elmustafa AA, Eastman JA, Rittner MN, Weertman JR, Stone DS. Scripta Mater 2000;43:951.
[15] Bhar DF, Kramer DE, Gerberich WW. Acta Mater 1998;46:3605.
[16] Mann AB, Pethica JB. Appl Phys Lett 1996;69:907.